Title

Paralytic, the Drosophila voltage-gated sodium channel, regulates proliferation of neural progenitors

Journal

Genes & Development, 33(23-24)

ISSN

0890-9369

Authors

Piggott, Beverly J
Peters, Christian J
He, Ye
et al.

Publication Date

2019-12-01

DOI

10.1101/gad.330597.119

Peer reviewed

Paralytic, the *Drosophila* voltage-gated sodium channel, regulates proliferation of neural progenitors

Beverly J. Piggott,[1,2] Christian J. Peters,[1,7] Ye He,[3] Xi Huang,[4,5,6] Susan Younger,[1,2] Lily Yeh Jan,[1,2] and Yuh Nung Jan[1,2]

[1]Department of Physiology, Department of Biochemistry and Biophysics, University of California at San Francisco, San Francisco, California 94158, USA; [2]Howard Hughes Medical Institute; [3]Neuroscience Initiative, Advanced Science Research Center, the Graduate Center, City University of New York, New York 10031, New York; [4]Program in Developmental and Stem Cell Biology, The Hospital for Sick Children, Toronto, Ontario, M5G 1X8, Canada; [5]Arthur and Sonia Labatt Brain Tumour Research Centre, The Hospital for Sick Children, Toronto, Ontario, M5G 1X8, Canada; [6]Department of Molecular Genetics, University of Toronto, Toronto, Ontario, M5S 3E1, Canada

Proliferating cells, typically considered "nonexcitable," nevertheless, exhibit regulation by bioelectric signals. Notably, voltage-gated sodium channels (VGSC) that are crucial for neuronal excitability are also found in progenitors and up-regulated in cancer. Here, we identify a role for VGSC in proliferation of *Drosophila* neuroblast (NB) lineages within the central nervous system. Loss of *paralytic* (*para*), the sole gene that encodes *Drosophila* VGSC, reduces neuroblast progeny cell number. The type II neuroblast lineages, featuring a population of transit-amplifying intermediate neural progenitors (INP) similar to that found in the developing human cortex, are particularly sensitive to *para* manipulation. Following a series of asymmetric divisions, INPs normally exit the cell cycle through a final symmetric division. Our data suggests that loss of Para induces apoptosis in this population, whereas overexpression leads to an increase in INPs and overall neuroblast progeny cell numbers. These effects are cell autonomous and depend on Para channel activity. Reduction of Para expression not only affects normal NB development, but also strongly suppresses brain tumor mass, implicating a role for Para in cancer progression. To our knowledge, our studies are the first to identify a role for VGSC in neural progenitor proliferation. Elucidating the contribution of VGSC in proliferation will advance our understanding of bioelectric signaling within development and disease states.

[*Keywords*: cancer biology; development; drosophila; neuroscience; proliferation; stem cells]

Supplemental material is available for this article.

Received July 10, 2019; revised version accepted October 28, 2019.

Neuronal excitability is a defining feature of nervous systems. Voltage-gated ion channels mediate changes in electrical potential (voltage) across cell membranes, triggering second messenger and gene regulatory cascades. Generation of these bioelectric signals is crucial for neuronal excitability, but their involvement in neurogenesis remains an open question. Expression of voltage-gated ion channels is often associated with differentiation in excitable tissues (Song et al. 2013; Francis et al. 2015; Li et al. 2019). However, bioelectric signals govern biology in every living cell type where the asymmetric distribution of ions across the plasma membrane establishes a membrane potential (Vm). Throughout development, tissues typically thought to be nonexcitable are subjected to changes in Vm, governing wide-ranging cell behaviors including proliferation, migration, differentiation, and death (McLaughlin and Levin 2018). The importance of bioelectric signals in nonexcitable tissues is evident as channelopathies include diseases that affect embryonic patterning and development, with consequences as severe as limb and craniofacial abnormalities (McLaughlin and Levin 2018).

The *Drosophila melanogaster* larval nervous system is a well-established model for elucidating mechanisms of neurogenesis (Doe 2008; Homem and Knoblich 2012; Homem et al. 2015; Farnsworth and Doe 2017). The ability of stem cells to preserve proliferation while generating

[7]Present address: Department of Anatomy and Cell Biology, University of Illinois at Chicago, Chicago, IL 60607, USA
Corresponding author: yuhnung.jan@ucsf.edu
Article is online at http://www.genesdev.org/cgi/doi/10.1101/gad.330597.119.

differentiated progeny is achieved through asymmetric division, a key feature of neuroblasts (the stem cells of the central nervous system in *Drosophila*). Some aspects of asymmetric division are conserved between *Drosophila* and humans and involve the segregation of fate determinants, whereby molecules for sustaining proliferation are segregated apically to be maintained in the neuroblast (NB), while molecular cues guiding differentiation are positioned basally, to be segregated into the daughter cell for its differentiation (Homem and Knoblich 2012). Disruption in the cell-type-specific expression of cell-fate determinants can lead to uncontrolled proliferation and brain tumors or insufficient neural populations. During larval development, NBs are found throughout the larval brain lobes and ventral nerve cord (VNC), and are identified by their patterns of division, genetic markings, and positions within the brain. NB progeny are distinguished by their positions and genetic markers. Type I neuroblasts express both Deadpan (Dpn) and Asense (Ase) and are found within the brain lobes and VNC where they asymmetrically divide to self-renew and generate a more differentiated, Ase^+, ganglion mother cell (GMC), which later symmetrically divides to generate two neurons or glia. Type II neuroblasts are Dpn^+ and Ase^-, they asymmetrically divide to generate an intermediate neural progenitor (INP). Once INPs mature, they become Ase^+ and Dpn^+ and they themselves asymmetrically divide to generate a symmetrically dividing GMC, which generates two neurons or glia (Bello et al. 2008; Boone and Doe 2008; Bowman et al. 2008). This INP transit-amplifying pattern of divisions in type II neuroblast populations, results in approximately 5×'s more neurons than the type I neuroblast lineage. The *Drosophila* larval nervous system thus provides a genetically tractable model to ask how ion channels influence cells in various states of proliferative potential and differentiation.

Previously, our laboratory has used *Drosophila* to characterize a role for the voltage-gated K^+ channel *ether-a-go-go* (EAG) in tumor development (Huang et al. 2012, 2015). In this study, we examine how the voltage-gated sodium channel (VGSC) governs aspects of neural development and tumor proliferation. Overexpression of the pore-forming α subunit of VGSC has been identified in cancers including breast cancer, cervical cancer, colon cancer, glioma, leukemia, lung cancer, lymphoma, melanoma, mesothelioma, neuroblastoma, ovarian cancer, and prostate cancer (Abdul and Hoosein 2002; Anderson et al. 2003; Fraser et al. 2005; Yang et al. 2012; Patel and Brackenbury 2015; Xia et al. 2016), implicating them in various aspects of cancer pathogenesis including migration, metastasis, invasion, and proliferation. Whether VGSC might also influence aspects of proliferation during normal development is not clear. There are nine genes for pore-forming VGSC α subunits in most mammalian genomes, but only a sole VGSC α subunit, *paralytic (para)* in *Drosophila*, making the latter a more straightforward model to investigate the in vivo role of VGSC in stem cell and tumor proliferation. We have identified a role for Para in regulating important aspects of neural progenitor proliferation in *Drosophila* larvae. Furthermore, we found that reduction of Para is sufficient to suppress brain tumor models driven by $Deadpan^{OE}$ (ectopic overexpression) (Zhu et al. 2012; Huang et al. 2015), activated Notch (Song and Lu 2011; Zhu et al. 2012), or knockdown of Brat (Bowman et al. 2008), indicating that Para may act downstream from genetic cascades that regulate important aspects of proliferation and differentiation.

Results

Reduction or loss of Para compromised proliferation of type I and type II neuroblast lineages

To examine the role of Para in brain development, we used RNAi to knock down *para* in the type I and type II neuroblast lineages using *inscuteable*-Gal4 (*insc*-Gal4). We found RNAi knockdown of *para* resulted in volume reduction of brain lobes but not the VNC (Fig. 1A–C). To assess the involvement of Para in type I and II neuroblast lineages, we generated a null allele of *para* using FLP recombinase of FRT insertion sites flanking the *para* gene region (method described in Supplemental Fig. S2A–E; Parks et al. 2004). As Para represents the sole VGSC in flies, its loss results in lethality (Broadie and Bate 1993). With MARCM (mosaic analysis with a repressible cell marker), we generated homozygous null clones marked by membrane bound mCD8-GFP within an otherwise heterozygous and viable animal (Lee et al. 1999). Compared with wild-type, $para^{-/-}$ MARCM clones had fewer cells per clone in both type I and type II neuroblast lineages (Fig. 1D–H; Supplemental Fig. S1D). MARCM only removed *para* within the clone, which suggested that Para acts cell autonomously in neuroblast lineage development. Indeed, cell-autonomous expression of *para* cDNA within the type I (Fig. 2A–D) or type II (Fig. 2G–J) neuroblast lineage was sufficient to rescue cell number in *para* null clones at 72 h after larval hatching (ALH), as well as at 96-h ALH (Supplemental Fig. S3). By examining cellular subtypes within $para^{-/-}$ MARCM clones, we found that loss of *para* significantly reduced the numbers of GMCs and neurons within type I clones, and this loss was rescued by Para cDNA expression (Fig. 2A′–C′,E,F). Similarly, loss of *para* significantly reduced the numbers of INPs, GMCs and neurons within type II MARCM clones, and this loss was rescued by *para* cDNA expression (Fig. 2G′–I′,K–M). Notably, the role of Para in neuroblast lineages may be more specific to central brain lineages as there was no significant difference found for medulla neuroblast lineages within the optic lobe (Supplemental Fig. S4A–C). As the cellular deficit was stronger within the type II lineage and progressively worsened over time (Fig. 1I), we decided to focus our studies of Para in the type II neuroblast lineage.

Type II $para^{-/-}$ *MARCM clones displayed a reduced rate of cellular accumulation*

To characterize cell loss in type II $para^{-/-}$ MARCM clones, we examined EdU (5-ethynyl-2′-deoxyuridine), a thymidine analog that is incorporated into DNA of

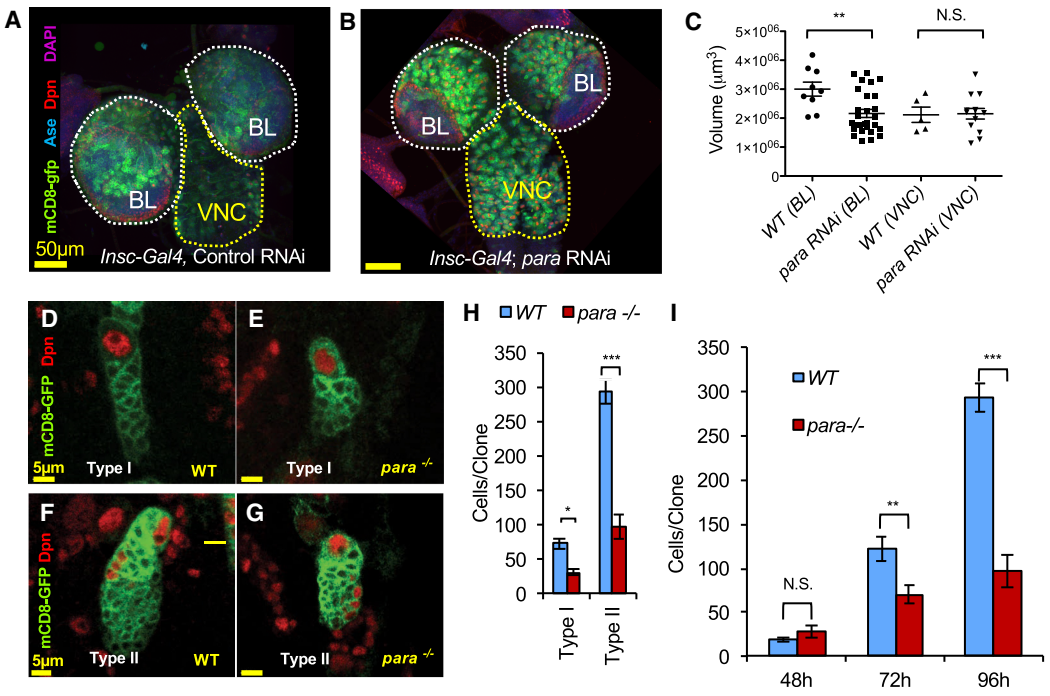

Figure 1. Reduction or loss of Para compromised proliferation of type I and II neuroblast lineages. (*A*) Representative image of wild-type larval central nervous system composed of two brain lobes (BL, white) and a ventral nerve cord (VNC, yellow) Scale bar, 50 µm. (*B*) RNAi knockdown of *para* in neural progenitors with *inscuteable* Gal-4 (*insc*-Gal4) in wild-type brains significantly reduced BL, but not VNC volume. Scale bar, 50 µm. (*C*) Two-tailed *t*-test, $P < 0.01$ BL: wild-type N = 9, *para* RNAi N = 28, VNC: wild-type N = 5, *para* RNAi N = 13 (*D*,*E*) Representative images of type I neuroblast wild-type and $para^{-/-}$ MARCM (mosaic analysis with a repressible cell marker) clones driven by enhancer trap *FLP recombinase 200c* (*ET-FLP 200C*) with *insc-Gal4* at 96 h (h) after larval hatching (ALH). Scale bar, 5 µm. (*F*,*G*) Representative images of type II wild-type and $para^{-/-}$ *ET-FLP 200c* MARCM clones. (*H*) $para^{-/-}$ type I and type II neuroblast MARCM clones had fewer cells per clone than wild-type. (type I: wild-type N = 14, $para^{-/-}$ N = 9, type II: wild-type N = 20, $para^{-/-}$ N = 26). Two-tailed *t*-test, $P < 0.05$. (*I*) Type II (*ET-FLP200c*) $para^{-/-}$ MARCM clones displayed similar cell numbers at 48 h after larval hatching (ALH), but at later time points, possessed progressively fewer cells per clone, compared with wild-type (48 h ALH: wild-type N = 19 $para^{-/-}$ N = 5, 72 h ALH: wild-type N = 15 $para^{-/-}$ N = 18, 96 h ALH: wild-type N = 20, $para^{-/-}$ N = 26). Scale bar, 5 µm.

dividing cells and labels newly generated progeny (Fig. 3A). Larvae were fed EdU for 4 h. Subsequently, we dissected these larvae either immediately (0 h) or 12 h off Edu. At the 0-h time point, most dividing cells (NB, INPs, GMCs) would be labeled (Fig. 3B,C′), whereas at 12 h off EdU, it would increasingly label post-mitotic cells as it was diluted from proliferating cells due to repeated cell division (Fig. 3D,E′). In wild-type type II MARCM clones, cell numbers increased over 12 h and, as expected, the number of EdU^+ cells increased as proliferation diluted EdU into progeny. However, in contrast to wild-type clones, the number of cells, as well as EdU labeled cells, was not significantly different from 0–12-h off EdU in $para^{-/-}$ clones (Fig. 3F,G). This suggests that type II $para^{-/-}$ MARCM progenitors either proliferated more slowly or have increased cell death.

Apoptosis is a major contributor to $para^{-/-}$ *type II lineage cell loss*

To determine whether $para^{-/-}$ cells undergo apoptosis, we made use of the baculovirus P35 to block apoptosis. During normal development, a significant proportion of type II neuroblast derived neurons die (Jiang and Reichert 2012). Here, blocking cell death in wild-type type II lineages led to a slight increase in cell number (Fig. 4A,C,D). In contrast, blocking apoptosis in type II $para^{-/-}$ MARCM clones dramatically increased the number of cells per clone (Fig. 4A,E,F). The cell number increase of P35 expressing $para^{-/-}$ clones, rescued $para^{-/-}$ cell number to a level similar to wild-type clones expressing P35 (Fig. 4A). These data suggested that the major driver of $para^{-/-}$ cell loss was due to apoptosis. We confirmed these findings by assessing cleaved caspase (cDCP-1) staining in type II lineages and found that RNAi knockdown of *para* reduced the number of cells per lineage and increased cDCP-1 labeled cells, indicating increased cell death upon reduction of Para (Supplemental Fig. 5A–F). While wild-type INP numbers were unchanged compared with wild-type clones expressing P35, $para^{-/-}$ clones expressing P35 had more INPs than those not expressing P35 (Fig. 4B,C′,F′). Consistent with this finding, knockdown of *para* in type II lineages leads to an increase in Ase^+cDCP1^+ labeled cells (Supplemental Fig. 5A′–C′,G), indicating that without Para, INPs and possibly GMCs underwent cell death. To investigate how INPs might be

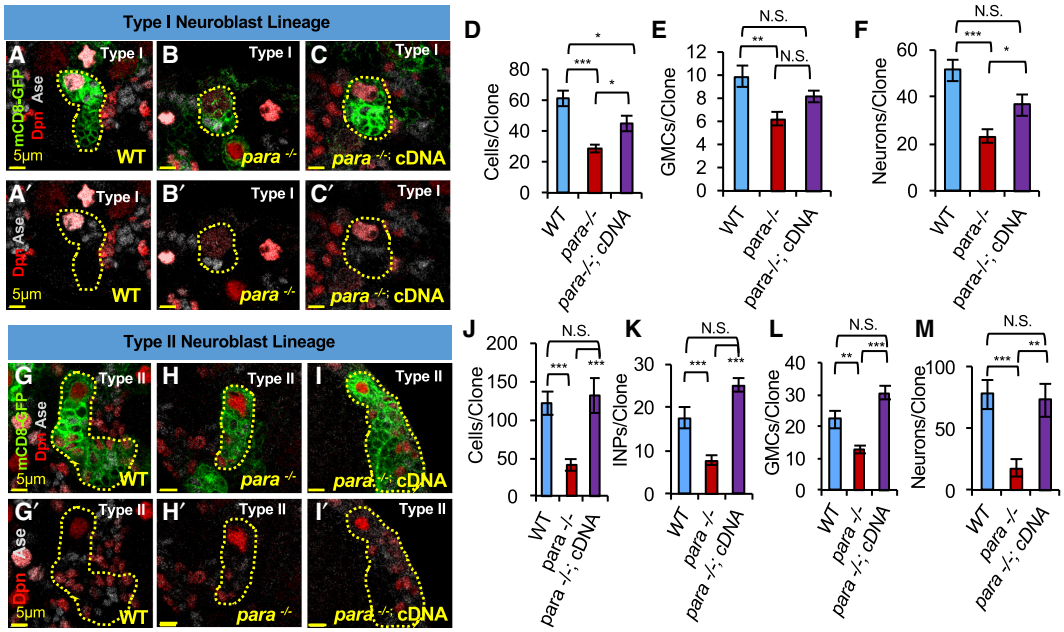

Figure 2. Cell loss in type I and II para$^{-/-}$ MARCM clones is rescued by cell-autonomous expression of para cDNA. (*A*–*C*′) Representative images of type I MARCM clones. (*A*′–*C*′) Type I progeny: NB are Dpn^{+}(red) and Ase^{+}(gray), GMCs are Ase^{+}. (*D*,*F*) *para*$^{-/-}$ MARCM clones have fewer cell numbers and cellular subtypes than wild-type and are rescued by cell autonomous *para* cDNA expression. Seventy-two hours ALH (Cells/lineage: wild-type N = 17 *para*$^{-/-}$ N = 20 *para*$^{-/-}$; cDNA N = 14, GMCs: wild-type N = 17, *para*$^{-/-}$ N = 16, cDNA N = 14, Neurons: wild-type N = 17, *para*$^{-/-}$ N = 14, cDNA N = 5. One-way ANOVA with Bonferroni multiple comparison test, $P < 0.05$) (*G*–*I*′) Representative images of type II MARCM clones. Type II progeny: NB are Dpn^{+}Ase^{-}, GMCs are Ase^{+}. (*J*–*M*) *para*$^{-/-}$ type II MARCM clones have fewer total cell numbers and cellular subtypes than wild-type and are rescued by cell autonomous expression of *para* cDNA. (Cells/lineage: wild-type N = 14 para$^{-/-}$ N = 19 *para*$^{-/-}$; cDNA N = 11, INPs: wild-type N = 14, *para*$^{-/-}$ N = 19, cDNA rescue N = 8, GMCs: wild-type N = 14, *para*$^{-/-}$ N = 18, cDNA N = 5 Neurons: wild-type N = 14, *para*$^{-/-}$ N = 18, cDNA N = 5. One-way ANOVA with Bonferroni multiple comparison test, $P < 0.01$) Clones driven by hs-FLP recombinase with *insc*-Gal4. Scale bar, 5 µm.

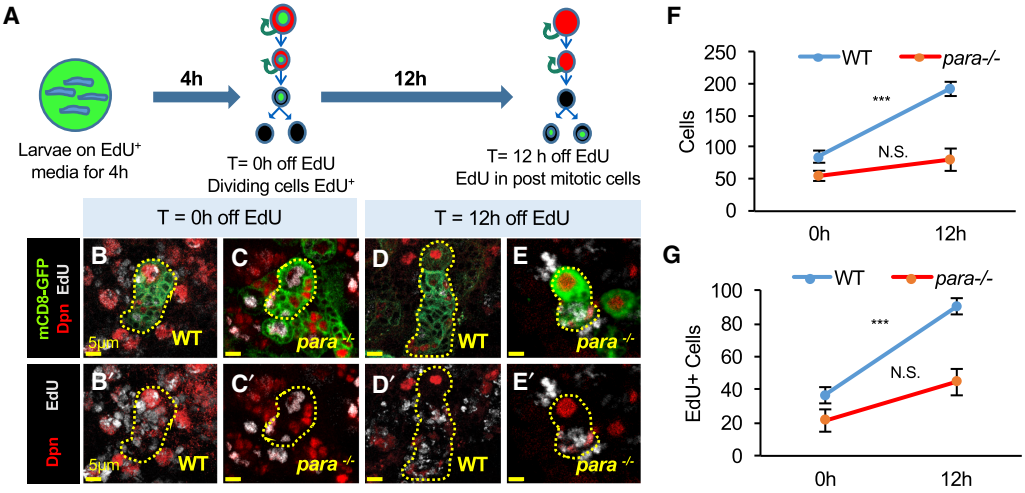

Figure 3. Type II *para*$^{-/-}$ MARCM clones displayed a reduced rate of cellular accumulation. (*A*) Schematic of EdU (5-ethynyl-2′-deoxyuridine) protocol. Seventy-two hours after larval hatching (ALH), larvae are are fed media mixed with EdU. (*B*–*E*′) Representative image of wild-type and *para*$^{-/-}$ MARCM clones (labeled by mCD8-GFP) at time = 0 h (*B*,*C*′) and t = 12 h off EdU (*D*,*E*′). At t = 0 h, EdU (gray) colocalizes with mitotically active, Dpn^{+} (red) neuroblasts (NBs) and intermediate progenitors (INPs), as well as in Dpn-ganglion mother cells (GMCs). (*D*,*E*′) Representative images of wild-type and *para*$^{-/-}$ MARCM clones at 12 h off EdU, where EdU is diluted from mitotically active (Dpn+) cells. (*F*) From 0 h to 12 h off EdU, wild-type total cell number increases, but *para*$^{-/-}$ MARCM cell numbers are not significantly changed from 0–12 h off EdU (wild-type: [0 h] N = 7, [12 h] N = 8, *para*$^{-/-}$: [0 h] N = 9, [12 h] N = 7, two-tailed *t*-test, $P < 0.001$). (*G*) From 0 h to 12 h off EdU, wild-type total number of EdU labeled cells increased, but EdU^{+} cell numbers are not significantly changed in *para*$^{-/-}$ MARCM clones (wild-type: [0 h] N = 7, [12 h] N = 7, *para*$^{-/-}$: [0 h] N = 9, [12 h] N = 7, two-tailed *t*-test, $P < 0.001$) Scale bar, 5 µm.

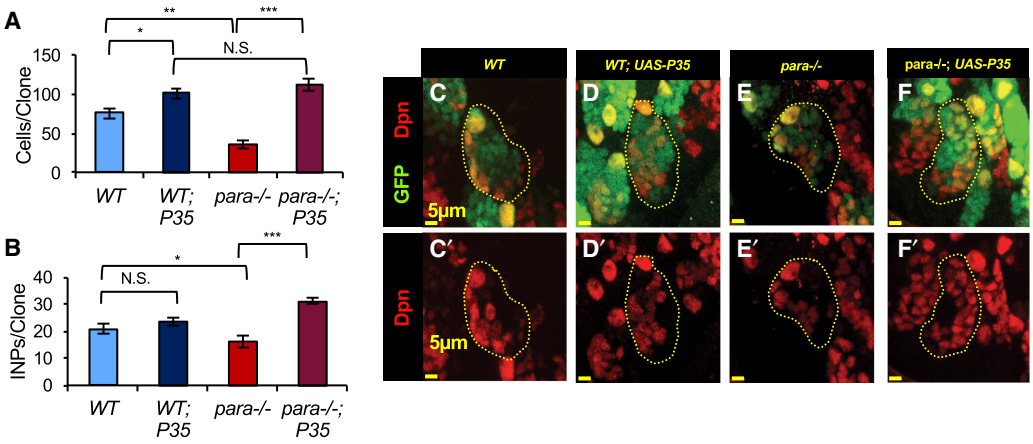

Figure 4. Apoptosis is a major contributor to *para*$^{-/-}$ type II lineage cell loss. (*A*) *Baculovirus* P35 was expressed within clones to block apoptosis. Expression of P35 slightly increased the number of wild-type cells, which likely reflects developmental apoptosis. Blocking apoptosis in *para*$^{-/-}$ type II MARCM clones rescues the number of cells to wild-type + *UAS-P35* levels (one-way ANOVA with Tukey multiple comparison test, $P < 0.05$. Wild-type N = 10 wild-type UAS-P35 N = 9 *para*$^{-/-}$ N = 6 *para*$^{-/-}$; UAS-P35 N = 8). (*B*) *para*$^{-/-}$ MARCM clones have fewer intermediate progenitors (INPs) than wild-type. Blocking cell death with P35 expression does not change the number of INPs in wild-type MARCM clones. Blocking cell death in *para*$^{-/-}$ MARCM clones increased the number of INPs, indicating that INPs are sensitive to apoptosis in *para*$^{-/-}$ MARCM clones (one-way ANOVA with Tukey multiple comparison test, $P < 0.05$. Wild-type N = 11 wild-type P35 N = 9 *para*$^{-/-}$ N = 9 *para*$^{-/-}$ P35 N = 8). (*C–F′*) Representative images of type II MARCM clones marked by GFP NLS (nuclear localized, GFP) in green and Dpn (red) to mark neuroblasts and INPs. Scale bar, 5 µm.

lost to apoptosis in *para*$^{-/-}$ clones, we used a cell cycle reporter (Supplemental Fig. S6A–C), and found an increased percentage of *para* null type II MARCM progeny (INPs and GMCs) in G2/M phase and a decreased percentage of cells in G1 as compared with wild-type (Supplemental Fig. S6E). As INPs and GMCs are much smaller than neuroblasts and thus more difficult to assess for DAPI condensed chromosomes, we stained for phosphohistone 3 (pH3), a M-phase marker, and found that an increased proportion of INPs are pH3+ and likely in M-phase (Supplemental Fig. S6F–H′). Conceivably, loss of Para could slow the cell cycle so as to increase the fraction of INPs in M-phase, in some cases resulting in cell cycle arrest that culminates in cell death. Loss of INPs would have cascading effects, diminishing the number of GMCs and neurons. There was also an enrichment of *para*$^{-/-}$ type II neuroblasts in G2 phase (Supplemental Fig. S6A–D), suggesting that these cells cycle more slowly than wild type. Additionally, as neural activity has been shown to be important for axon guidance and synaptic refinement (Casagrande and Condo 1988; Patel and Brackenbury 2015), and loss of $Na_V1.2$ results in marked increases in neuronal apoptosis (Planells-Cases et al. 2000), a proportion of *para*$^{-/-}$ neurons may be expected to die from apoptosis. While we did not see increased cDCP1 staining within neurons (Supplemental Fig. 5H), *insc*-Gal4 was more strongly expressed in NBs and INPs. Moreover, when a more direct neuronal Gal4 was used (*elav*-Gal4), no progeny arose, indicating that neuron-specific *para* knockdown is lethal as has been previously reported (data not shown and Parker et al. 2011). Thus, we cannot exclude the possibility that neuronal cell death may occur with a more complete reduction of Para or at other time points. These data indicated that loss of Para within MARCM clones led to fewer cells due to apoptosis of neuroblast progeny that potentially arose from cell cycle arrest and may have minor contributions from a slower cell cycle of neuroblasts and neural progenitors.

Overexpression of Para increased cell number in type II NB lineages

Having found that loss of Para reduced cell number in neuroblast lineages, we examined the effect of increasing Para expression in an otherwise wild-type lineage. To this end, we overexpressed a wild-type *para* cDNA as well as a *para* gain of function allele, *bang senseless* (BSS), which is thought to cause hyperexcitability via a shift of fast inactivation towards more positive potentials (Parker et al. 2011). *bang senseless* was identified as a seizure prone mutant upon mechanical stimulation (Ganetzky and Wu 1982) and later attributed to the missense mutation L1699F, a region highly conserved with mammalian VGSC, within the *para* locus (Parker et al. 2011). Overexpression of *para* cDNA in the type II neuroblast lineage, using *insc*-Gal4 with *ase*-Gal80, increased the number of cells per lineage compared with wild type at the same time point (Fig. 5A–D). There was no significant difference between wild-type *para* cDNA overexpression and *bss* cDNA overexpression (Fig. 5D). Notably, INP numbers were increased in *para* cDNA overexpressing lineages compared with wild-type, indicating that increased expression of Para may lead to faster proliferation of type II neuroblasts or longer lifespans of INPs (Fig. 5A′–C′,E). Consistent with the idea that INPs may be regulated by Para, altering Para expression levels with RNAi knockdown (Supplemental Fig. 7A–F) or by overexpression of *para* cDNA in INPs alone was sufficient to

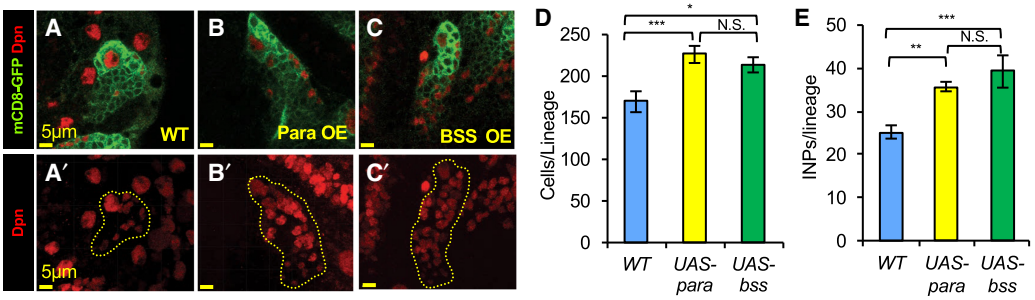

Figure 5. Overexpression of para cDNA increased cell number in wild-type type II lineage. (*A–C*) Representative image of wild-type and *para* cDNA overexpression within type II lineages marked by mCD8-GFP (green) and stained for Dpn (red). (*A′–C′*) Maximum projections of wild-type or *para* cDNA overexpression in type II cellular lineage to show Dpn+ NB and INPs within lineages. (*D*) Overexpression of wild-type cDNA labeled Para OE (Para Over Expression) or hyperactive $para^{L1699F}$mutant known as, *bang senseless* (BSS OE), driven by *incuteable*-Gal4; *asense*-Gal80, increased the number of cells per clone, to a similar extent, compared with wild-type at 96 h ALH (wild-type N = 13, Para wild-type cDNA N = 15 wild-type BSS cDNA N = 12. One-way ANOVA with Bonferroni multiple comparison test, $P < 0.05$). (*E*) Overexpression of *para* or *bss* cDNA in type II lineages, similarly, showed more Dpn^+ INPs than wild-type (wild-type N = 18, Para wild-type cDNA N = 12 wild-type BSS cDNA N = 5. One-way ANOVA with Bonferroni multiple comparison test, $P < 0.01$). Scale bar, 5 μm.

decrease or increase INP number as well as the numbers of GMCs and neurons, respectively (Supplemental Fig. 7G–L). Thus, Para expression likely influences NBs as well as INPs.

Reduction of Para suppressed brain tumor size

Having found that the abundance of Para influences proliferation in neuroblast lineages, we asked whether reduction of Para can influence overproliferation within a brain tumor. Deadpan (Dpn) is a bHLH (basic-helix-loop-helix) transcriptional repressor expressed in neuroblasts of embryonic and larval brains, as well as intermediate neural progenitors (Fig. 6A,A″; Bier et al. 1992; Younger-Shepherd et al. 1992). Overexpression of Dpn in the type I and type II neuroblast lineage, driven by *insc*-Gal4, led to brain tumor formation in *Drosophila* larval brains as a result of overproliferation (Fig. 6B,B″,D,D″,F,G; Zhu et al. 2012). RNAi knockdown of *para* within a Dpn^{OE} tumor resulted in a reduction in size of both the brain lobes and VNC (Fig. 6C,C″,E,E″,F,G).

A recent study examined the crystal structure of Brat, a translational repressor, in complex with RNAs. Brat is involved in direct differentiation of neuronal stem cells by suppressing self-renewal factors, and it binds known proliferation factors including *chinmo*, *dpn*, *klu*, *staufen* (*stau*), and *par-6* mRNAs (Loedige et al. 2015). An unexpected finding was that Brat was also found in complex with *para* mRNA, suggesting a potential influence of the sole *Drosophila* VGSC in promoting stemness. To ask whether Para may have a more generalized role in proliferation, we generated type II neuroblast derived tumors with genes involved in developmental pathways known to influence neuroblast lineage self-renewal and differentiation. Overexpressing Dpn (DpnOE) (Zhu et al. 2012) or overexpressing activated Notch (N^{IC}) (Song and Lu 2011; Zhu et al. 2012), or knockdown of Brat (Bowman et al. 2008) with *insc-Gal4* with *ase-Gal80* was sufficient to generate type II brain tumors (Fig. 6H–J). Introducing a hypomorphic *para* mutant, $para^{TS1}$, in these tumors led to a profound reduction in tumor size (Fig. 6K–N). Together these data indicate that Para promoted brain tumor growth derived from both type I and II lineages, as its reduction suppressed brain tumor mass. $para^{TS1}$ suppression of tumors generated by manipulating Dpn, Notch, and Brat signaling suggests that it regulates proliferation downstream from important developmental cascades (Supplemental Fig. S8D).

Para channel activity is important for its role in type II neuroblast lineage development

We next asked whether the involvement of Para in development depended on its function as a channel. Para is a pore forming α subunit member of the VGSC family; it contains four homologous domains (DI-DIV) each with six transmembrane segments (Fig. 7A; Catterall 2000). VGSCs are closed at the resting membrane potential. Upon membrane depolarization, VGSCs are activated through outward movement of the S4 voltage sensors. After a few milliseconds, VGSCs inactivate through an inactivation gate found within the intracellular loop connecting domains III and IV (Catterall 2000).

To address whether the Para ion channel activity was important in development, we examined a lethal point mutant $para^{V1401E}$ (Yamamoto et al. 2014). Valine 1401 lies within the intracellular loop between S4 and S5 of domain III (Fig. 7A), where the change from a hydrophobic valine to a hydrophilic glutamate may result in misfolding or interfere with voltage gating. In addition, residues within this intracellular loop IIIS4-S5 may stabilize the inactivation gate, whereby mutations in this region impair inactivation (Smith and Goldin 1997; Catterall 2000). We found that homozygous MARCM clones of $para^{V1401E}$ displayed fewer cells per clone and phenocopied $para^{-/-}$ MARCM clones (Fig. 7B). As this mutant allele had not been electrophysiologically characterized, we performed two-electrode voltage clamp recordings of wild-type

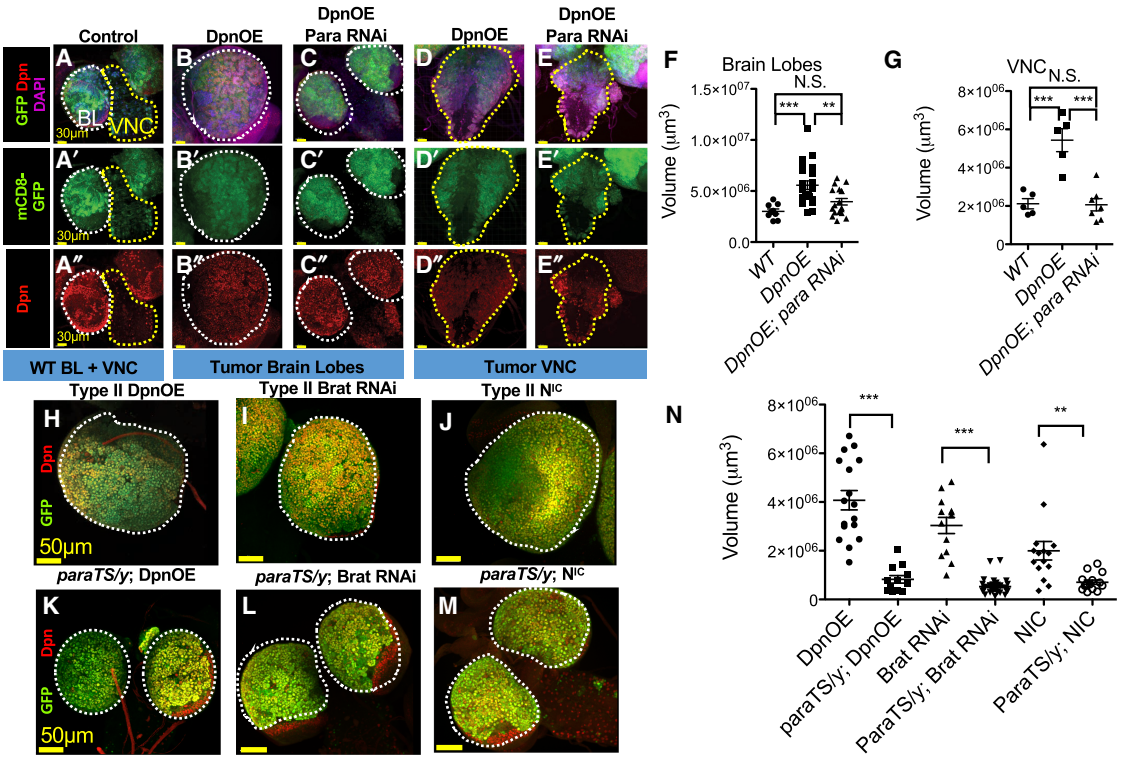

Figure 6. Reduction of Para expression suppressed *Drosophila* brain tumors. (*A*,*A*″) Representative image of wild-type brain lobes (BL) and ventral nerve cord (VNC). Scale bar, 30 µm. (*B*,*B*″,*D*,*D*″) Ectopic overexpression of Dpn (DpnOE), driven by *insc*-Gal4, led to expansion of Dpn+ (red) cells (*B*″) and generation of a brain tumor with enlarged brain lobes (*B*,*B*″ and *F*) and VNC (*D*,*D*″ and *G*). Scale bar, 30 µm. (*C*, *C*″ and *E*,*E*″) *para* RNAi knockdown in DpnOE brain tumor reduced BL size (*F*) and VNC volume (*G*). One-way ANOVA with Tukey multiple comparison test, *P*-value < 0.05 (BL: DpnOE, N = 21, DpnOE *para* RNAi, N = 17) and (VNC: DpnOE, N = 5, DpnOE *para* RNAi, N = 8). (*H*–*J*) Representative image of BL, type II brain tumors driven by *insc*-Gal4 with *Asense*-Gal80 (nuclear localized green fluorescent protein [GFP] for volume measurement). (*H*) Type II DpnOE brain tumor, (*I*) Brat brain tumor, generated by Brat RNAi knockdown, (*J*) Notch (N^{IC}) brain tumor generated by overexpression of activated Notch. (*K*–*M*) Representative image of hypomorphic $para^{TS1}$ mutants reduced type II brain tumors. Scale bar, 50 µm. (*N*) Two-tailed *t*-test, (**) $P < 0.001$ (BL: DpnOE, N = 17, $para^{TS1}/y$, N = 12, Brat, N = 13, $para^{TS1}/y$;*Brat*, N = 37, N^{IC}, N = 17, $para^{TS1}/y$; N^{IC}, N = 12).

para and $para^{V1401E}$ mutant channels heterologously expressed in *Xenopus* oocytes. The *tipE* β subunit was coinjected in a 1:1 molar ratio to stabilize expression (Feng et al. 1995; Warmke et al. 1997). Current-voltage (I-V) relationships were obtained from a holding potential of −80 mV. Wild-type Para channels demonstrated a mean peak current amplitude at 0 mV of −0.87 ±0.11 µA (Fig. 7C; Supplemental Fig. S9A). The V1401E mutant channels displayed a significant reduction in current amplitude, with a mean peak of −0.11 ±0.01 µA (Fig. 7C; Supplemental Fig. S9B). In order to probe whether Na^+-flow or some other property of Para protein was responsible for the phenotypes, we designed a "pore dead" construct based on homology with $Na_V1.2$. To this end we performed a full protein sequence alignment (ClustalΩ) of Para with rat $Na_v1.2$ (NP_036779.1) and identified a single aspartate residue, D388, with asparagine. This residue contributes to the conserved ion conduction pore among Na_v family members (Fig. 7A), and mutation to asparagine results in reduced sodium conductance while preserving surface expression of the channel (Pusch et al. 1991). When expressed in oocytes, D388N mutant channels yielded currents with a mean peak current amplitude of −0.07 ± 0.01 µA (Fig. 7C; Supplemental Fig. S9C).

These results suggested that $para^{V1401E}$ had impaired channel function and, as it phenocopied complete loss of Para, that channel function was likely important for the contribution of Para to the development of neuroblast lineages. We therefore asked whether the nonconducting D388N mutant channel would rescue $para^{-/-}$ MARCM clones and whether its overexpression in the type II wild-type lineage would mimic the increased cell number seen with wild-type *para* cDNA. $para^{D388N}$ cDNA was not able to rescue $para^{-/-}$ MARCM clone cell numbers (Fig. 7D,F–I), nor increase the number of cells per type II neuroblast lineage (Fig. 7E,J–L), suggesting that the ability of Para to conduct Na^+ ions is important for its role in neuroblast development.

Discussion

VGSCs play important roles during neural development where neural activity is important for axon guidance

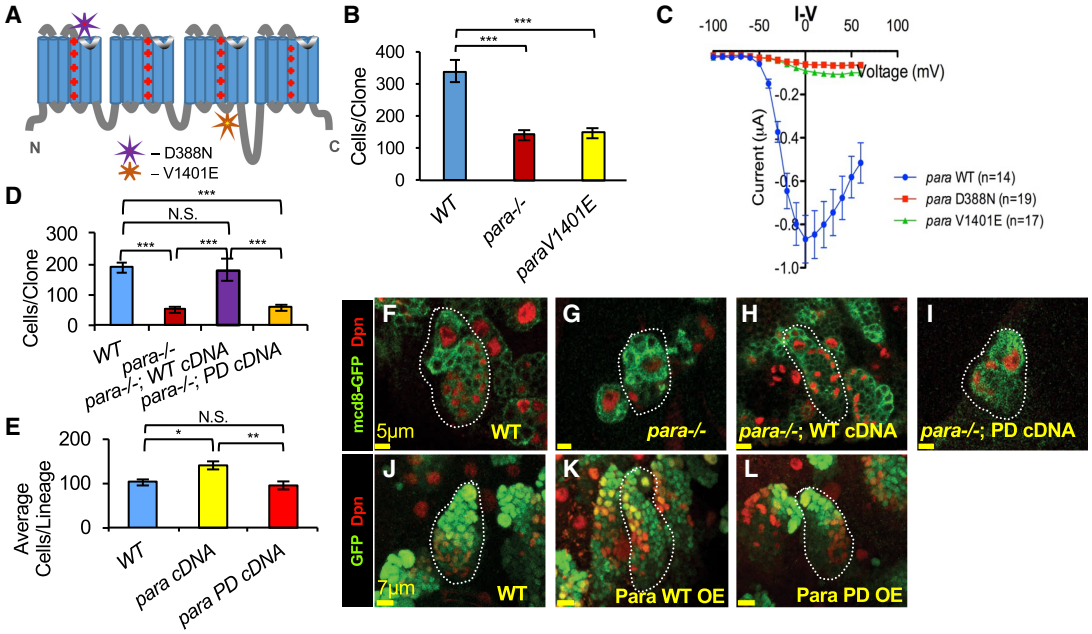

Figure 7. Para channel activity is important for its role in type II neuroblast lineage development. (*A*) Cartoon of Para protein structure with relative location of missense point mutants. (*B*) *para*^{V1401E} phenocopied *para*$^{-/-}$ type II MARCM clones, with fewer cells per clone compared with wild-type, at 96 h after larval hatching (ALH). (One-way ANOVA with Tukey's multiple comparison test, [***] $P < 0.0001$. Wild-type N = 19 *para*$^{-/-}$ N = 20 *para*^{V1401E} N = 29). (*C*) Whole-cell Na^+ currents in cRNA-injected oocytes were measured using a two-microelectrode voltage clamp to examine the current–voltage relationship (*I-V* curves) of wild-type versus V1401E and a D388N mutation (nonconducting or pore dead [PD]) (*C*). Wild-type Para currents are inward rectifying, while V1401E and a D388N display little to no current wild-type: N = 14 V1401E N = 16 D388N N = 19. (*D*) Unlike wild-type *para cDNA*, PD cDNA was unable to rescue type II *para*$^{-/-}$ cell deficit. (One-way ANOVA with Tukey's multiple comparison test, (***) $P < 0.0001$ wild-type N = 6 *para*$^{-/-}$ N = 8 *para*$^{-/-}$ wild-type cDNA N = 5 *para*$^{-/-}$ D388N cDNA N = 5). (*F–I*) Representative images of type II MARCM clones labeled by mCD8-GFP and Dpn^+ (red). Scale bar, 5 µm. (*E*) Unlike wild-type *para* cDNA, overexpression of *para*^{D388N} mutant cDNA did not increase type II cell number. (One-way ANOVA with Tukey's multiple comparison test, (***) $P < 0.05$ wild-type N = 6 wild-type cDNA OE N = 7 D388N cDNA OE N = 9). (*J–L*) Representative images of type II MARCM clones marked by nuclear localized GFP. Scale bar, 7 µm.

and synaptic refinement (Casagrande and Condo 1988; Subramanian et al. 2012). VGSC activity within the nervous system is essential, as its absence leads to lethality in a number of mouse models (Harris and Pollard 1986; Planells-Cases et al. 2000; Yu et al. 2006). In addition, mutations in VGSC are associated with childhood diseases including autism spectrum disorders, epilepsy, mental retardation, among others, highlighting the necessity for understanding the role of VGSC during development (Eijkelkamp et al. 2012).

Recent work has begun to uncover functions of VGSC in development of nonexcitable cells. One such study found that $Na_V1.3$ channels (encoded by SCN3A) are expressed in radial glial cells and are important for migration during cortex development (Smith et al. 2018). A large scale clinical study has found that 25% of individuals with SCN2A mutations presented with microcephaly (Stessman et al. 2017), suggesting that VGSC may influence neuronal progenitor proliferation. Additionally, VGSCs are important for cardiac progenitor development in zebrafish (Chopra et al. 2010). These studies indicate that VGSCs play a role in progenitors during development, although the nature of their contributions is unclear.

In this study, we identified a role for the VGSC Para in neural development. We found that loss of *para* reduced total cell number in the type I and type II central neuroblast lineages. These effects are cell autonomous and could be rescued by cDNA expression within neuroblast lineages. The stronger phenotype observed in the type II lineage may reflect a role for Para in INPs, which are only present in the type II lineage (Supplemental Fig. S8A,B).

Loss of Para led to increased apoptosis that may arise from a failure of cell cycle progression. Research in other systems has found that depolarization is essential for G2 to M progression (Blackiston et al. 2009) and it is possible that Para promotes cell cycle progression in *Drosophila* progenitors through its depolarizing activity (Supplemental Fig. S6B). Proliferative cells tend to display more depolarized resting membrane potentials, as compared with differentiated cells, like neurons (Yang et al. 2012). In this context, Para may primarily exist in the inactivated state and a persistent sodium current of an amplitude significantly smaller than that of the transient current, may predominate. In addition, VGSCs are highly subjected to RNA editing and alternative splicing. Some of these variants result in window currents and persistent currents,

like that found in embryonic variants of Para (Lin et al. 2009). Para could, therefore, contribute to a depolarized state that may be important for proliferation. Alternatively, Para could be temporally up-regulated during specific states of the cell cycle to activate downstream molecular cascades. Depolarization has been shown to influence cell cycle regulation, including gene expression, calcium signaling, protein localization, and phosphorylation states (Abdul Kadir et al. 2018; McLaughlin and Levin 2018). The contribution of VGSC to axon growth cones, metastasis, and migration indicates a role for depolarization in cytoskeletal rearrangement (Patel and Brackenbury 2015). The cytoskeleton contributes to many aspects of cell division including subcellular localization of cell-fate determinants during asymmetric cell division, volume changes, nuclear envelope breakdown, and chromosome segregation during M-phase (Betschinger and Knoblich 2004; Hutterer et al. 2004; Homem and Knoblich 2012). If Para activity were to influence any of these processes, dysregulation of cell cycle progression would be expected.

VGSCs drive membrane depolarization as they catalyze selective permeation of sodium ions, thereby driving the membrane potential towards the sodium equilibrium potential. A number of studies highlight the potential role of Na^+ signaling as a driver of proliferation. Regeneration experiments in *Xenopus laevis* find $Na_V1.2$ mediated Na^+ influx, rather than depolarization, acts through salt inducible kinase (SIK) to drive proliferation, outgrowth, and morphogenesis by activating Notch, Wnt, BMP, and FGF signaling (Tseng et al. 2010). Moreover, a number of recent studies in *Drosophila* find that sodium permeable ion channels promote proliferation. These include the epithelial sodium channel ENaC whose overexpression drives gut stem cell overproliferation (Kim et al. 2017), ROS stimulated upregulation of cation permeable TRPA1 channels that induce proliferation (Xu et al. 2017), and cation permeable Piezo that is important for proliferation in the adult fly midgut (He et al. 2018) as well as glioma proliferation in multiple fly glioma model (Chen et al. 2018).

Our studies have identified a role for voltage-gated sodium channel, Para, in neural development and cancer. Going forward it will be interesting to discover how the activity of other ion channels, exchangers and pumps converge to influence cellular behavior. While Para's actions were cell autonomous, it's intriguing to wonder whether signaling within progeny and the cellular niche occurs. Many progenitors are connected through gap junctions and electrical signaling likely facilitates communication and coordination, essential for tissue patterning and cellular morphogenesis during development and regeneration. Genetically tractable model systems like *Drosophila* provide a platform to build this knowledge and further our understanding of the contribution of ion channels to proliferation and differentiation. VGSCs are promising sites for therapeutic intervention due to their druggable structure and the availability of FDA approved medications targeting them for pain and antipsychotics (Patel and Brackenbury 2015). These studies will offer significant insight towards future biomedical therapies for birth defects, cancer and regenerative medicine.

Materials and methods

Drosophila *stocks*

UAS-dpn (Wallace et al. 2000; Zhu et al. 2012) *Insc-Gal4; Ase-Gal80* (Zhu et al. 2012). *UAS-para RNAi* (BL31676 y^1 v^1; P{TRiP.JF01469}attP2) or y1 sc* v1 sev21; P{TRiP.HMS00868}attP2 and control stock y^1 v^1; P{UAS-GFP.VALIUM10}attP2 (BL35786) or y1 v1; P{UAS-LUC.VALIUM10}attP2 (BL35788) were crossed to w* *UAS-mCD8-GFP; insc-GAL4,UAS-dcr2/CyO, tubG80*; UAS-Dpn. Or w*, UAS-mCD8-GFP; r9d11-Gal4. $para^{ts}$ (Ganetzky 1984) $para^{ts1}$*; insc-GAL4, UAS-GFP*^{NLS}*/CyO,weep, and* control *w**; *insc-GAL-4,UAS-GFP*^{NLS}*/CyO, weep*, crossed to males *UAS-dpn/TM6B,tb* or $para^{ts1}$*;UAS-dpn/TM6B,Tb*, or activated Notch designated N^{IC} *(BL5830) w-, UAS-*$^{N\Delta B2A2}$or brat RNAi knockdown tumor: y^1 sc* v^1 sev^{21}; P{TRiP.HMS01121}attP2. MARCM analysis stocks: *w* HS-FLP FRT19A; Insc-Gal4, UAS-mCD8-GFP* or w^- *HS-FLP FRT19A; Insc-Gal4, UAS-GFP*^{NLS} or *w- HS-FLP FRT19A; Insc-Gal4, UAS-td-tomato* crossed to control *w* FRT19A* or mutants *w* para*$^{-/-}$ *FRT19A/FM7, Kr-Gal4*, UAS-GFP. Rescue experiments: *w- para*$^{-/-}$ *FRT19A/FM7, Kr-Gal4*, UAS-GFP; *UAS-para* (*UAS-para*, aka UAS-DmNaV, (gift from Marc Tanoyue), and *w* para*$^{-/-}$ *FRT19A/FM7, Kr-GAL4*, UAS-GFP; *UAS-para*^{D388N}*/CyO, Kr-Gal4*, UAS-GFP. What we refer to as *para*^{V1401E} *(y^1 w* para*^{B}*/FM7, Kr-GAL4*, UAS-GFP [BL57109]). FUCCI analysis: *w1118; P{UAS-GFP.E2f1.1-230}32P{UAS-mRFP1.NLS.CycB.1266}19/CyO, P{en1}wgen11; MKRS/TM6B, Tb1 (BL55121)*, w^{1118} FRT19A; FUCCI/CyO,weep or *w*^{1118}*para*$^{-/-}$*FRT19A; FUCCI/CyO, Weep* cossed with: *w* HS-FLP FRT19A; Insc-GAL4*.

Generation of para *null allele*

PBac{WH}f04029 (Exelixis:f04029 at Harvard Medical school) and *P{XP}para*^{d04188} (Exelixis:d04188 from Harvard Medical School) stocks were used to generate a deletion of the Para gene region. FLP recombinase and FRT-bearing insertion was used to generate an isogenic deletion with molecularly defined endpoints described in Parks et al. (2004). To assess loss of Para gene region, a reverse primer within an intron: CTGCTGTATTCGAGT CATTGG and a forward primer within a coding region: TTCGGATGGGCTTTCCTGTC generate a 500-bp band.

MARCM clones

Mosaic analysis with a repressible cell marker (MARCM) neuroblast clones were generated similar to previously described (Lee et al. 1999). Dissections occurred at 48, 72, and 96 h after larval hatching. In addition to *HS-FLP recombinase,* we also used an enhancer-trap recombinase, *FINGR-FLP* (*ET-FLP 200c*) (Bohm et al. 2010) without heat shock, but with similar collection and dissection times.

cDNA Para over expression analysis

UAS-*para* and UAS-*para*^{bss} from Parker et al. 2011). UAS-*para*^{D388N} was generated by introducing the D388N point mutation into a wild-type cDNA (Olson et al. 2008). *para*^{D388N} cDNA was inserted into the VK37: (2L) 22A3 PhiC31 site fly stock.

Drosophila immunohistochemistry and microscopy Larval brains were dissected, fixed, and stained similarly to previously described (Zhu et al. 2012). Primary antibodies: guinea pig anti-Ase (1:1000), rabbit anti-Dpn (1:500) rat anti-cd8 GFP (1:400 from invitrogen 13-0081-82), rat anti-tdtom (Kerafast EST203), chicken anti-GFP (1:400 from Aves laboratory GFP-1020) chicken

anti-mcherry (1:400 from Novus biologics NBP2-25158). Cleaved Caspase staining (rabbit anticleaved DCP-1) (1:200; Asp216, Cell Signaling Technology 9578S). Secondary antibodies: Alexa Fluor 488 (Invitrogen A-11006), Alexa Fluor 555 (A-21428), or 633(A-21105) (Invitrogen) were used at 1:400 and DAPI staining at 1:1000. Before imaging, brains were mounted onto slides with vectashield and coverslipped. Imaging was preformed using either Leica SP5 or Leica SP8. Brain tumor images were acquired with 1-µm stacks. MARCM clones and type II lineages were acquired with 0.5-µm stacks. Imaris 5.5 software was used for volume measurement and cell counting.

Edu labeling and staining

Seventy-two hour ALH staged larvae were placed on kankel-white medium containing 0.2 mM EdU and bromophenol blue for 4 h. After 4 h, half of the larvae were dissected at 0 h or 12 h later off EdU. EdU (5-ethynyl-2′-deoxyuridine) labeling protocol is described in Daul et al. (2010). Click-iT Plus EdU Alexa Fluor 647 Imaging Kit was used as described in the manufacturer's protocol (Thermo Scientific C10640). Rat anti cd8 (1:400), rabbit anti Dpn (1:500) primary antibody solutions were diluted in blocking buffer and incubating overnight at 4°C. Secondary labeling continued the next day as described above.

Xenopus *oocyte recording and RNA preparation*

For oocyte expression, 1 µg PGH19 plasmid DNA containing the DmNaV (a gift from Ke Dong's laboratory) (Olson et al. 2008) was linearized using the NotI and in vitro transcribed to cRNA with T7 polymerase (mMESSAGE mMACHINE kit, Ambion AM1344). cRNA for *Drosophila tipE* cRNA, enhances Para expression, was prepared similarly (Feng et al. 1995; Warmke et al. 1997). Oocytes were harvested from *Xenopus laevis* frogs in accordance with protocols approved by the Institutional Animal Care and Use Committee at UCSF. Manually separated and enzymatically defolliculated stage V-VI oocytes were injected with 50 nL of up to 200 ng/uL of mRNA encoding wild-type or mutant *para* plus *tipE* mRNA in a 1:1 ratio. Oocytes were subsequently maintained at 18°C with gentle agitation in ND96 containing, in mM: 96 NaCl, 3 KCl, 1 $MgCl_2$, 2 $CaCl_2$, and 5 HEPES (pH 7.4/NaOH) supplemented with 100 units/mL penicillin, 100 µg/mL streptomycin, and 50 µg/mL gentamicin.

Two electrode voltage clamp electrophysiology and data analysis

Forty-eight to 72 h after injection, oocytes were transferred to a recording bath containing antibiotic-free ND96, impaled by with two borosilicate electrodes (R = 0.2–1.0 MΩ) filled with 3 M KCl and clamped to an initial holding potential of −80 mV using a GeneClamp 500B amplifier and Digidata 1320A digitizer (Axon Laboratories) driven by pClamp10. Individual sweeps were sampled at 20 kHz and subjected to 6× P/N subtraction online, then low-pass filtered off-line using an 8-pole Bessel filter at 2 kHz. Nonnormalized antipeak values from each sweep and averaged to generate I/V curves, and are presented as mean ±SEM, with n values representing total number of individual cells taken from at least four separate days of recording.

Acknowledgments

We thank Ruijun Zhu, Ke Li, Caitlin O'Brien, Jacob Jaszczak, Han-Hsuan Liu, David Crottes, Maja Petkovic, Mu He, Chin Fen Teo, Cindy Li, and other Jan laboratory members for helpful discussions and experimental consultations. We thank Mark Tanoyue (UC Berkeley) for generous gifts of fly stocks and Ke Dong (Michigan State University) for generous gifts of *para* cDNA and helpful input on culturing conditions. Stocks obtained from the Bloomington Drosophila Stock Center (NIH P40OD018537) were used in this study. Funding was provided by a Lefkofsky foundation Damon Runyon Cancer Research Foundation Fellowship (B.J.P.) and National Institutes of Health (NIH) grant 1R35NS97227 to Y.N.J. Y.N.J. and L.Y.J. are investigators at the Howard Hughes Medical Institute.

References

Abdul M, Hoosein N. 2002. Voltage-gated sodium ion channels in prostate cancer: expression and activity. *Anticancer Res* **22:** 1727–1730.

Abdul Kadir L, Stacey M, Barrett-Jolley R. 2018. Emerging roles of the membrane potential: action beyond the action potential. *Front Physiol* **9:** 1661. doi:10.3389/fphys.2018.01661

Anderson JD, Hansen TP, Lenkowski PW, Walls AM, Choudhury IM, Schenck HA, Friehling M, Höll GM, Patel MK, Sikes RA, et al. 2003. Voltage-gated sodium channel blockers as cytostatic inhibitors of the androgen-independent prostate cancer cell line PC-3. *Mol Cancer Ther* **2:** 1149–1154.

Bello BC, Izergina N, Caussinus E, Reichert H. 2008. Amplification of neural stem cell proliferation by intermediate progenitor cells in *Drosophila* brain development. *Neural Dev* **3:** 5. doi:10.1186/1749-8104-3-5

Betschinger J, Knoblich JA. 2004. Dare to be different: asymmetric cell division in *Drosophila*, *C. elegans* and vertebrates. *Curr Biol* **14:** R674–R685. doi:10.1016/j.cub.2004.08.017

Bier E, Vaessin H, Younger-Shepherd S, Jan LY, Jan YN. 1992. *deadpan*, an essential pan-neural gene in *Drosophila*, encodes a helix-loop-helix protein similar to the *hairy* gene product. *Genes Dev* **6:** 2137–2151. doi:10.1101/gad.6.11.2137

Blackiston DJ, McLaughlin KA, Levin M. 2009. Bioelectric controls of cell proliferation: ion channels, membrane voltage and the cell cycle. *Cell Cycle* **8:** 3527–3536. doi:10.4161/cc.8.21.9888

Bohm RA, Welch WP, Goodnight LK, Cox LW, Henry LG, Gunter TC, Bao H, Zhang B. 2010. A genetic mosaic approach for neural circuit mapping in *Drosophila*. *Proc Natl Acad Sci* **107:** 16378–16383. doi:10.1073/pnas.1004669107

Boone JQ, Doe CQ. 2008. Identification of *Drosophila* type II neuroblast lineages containing transit amplifying ganglion mother cells. *Dev Neurobiol* **68:** 1185–1195. doi:10.1002/dneu.20648

Bowman SK, Rolland V, Betschinger J, Kinsey KA, Emery G, Knoblich JA. 2008. The tumor suppressors Brat and Numb regulate transit-amplifying neuroblast lineages in *Drosophila*. *Dev Cell* **14:** 535–546. doi:10.1016/j.devcel.2008.03.004

Broadie K, Bate M. 1993. Activity-dependent development of the neuromuscular synapse during *Drosophila* embryogenesis. *Neuron* **11:** 607–619. doi:10.1016/0896-6273(93)90073-Z

Casagrande VA, Condo GJ. 1988. The effect of altered neuronal activity on the development of layers in the lateral geniculate nucleus. *J Neurosci* **8:** 395–416. doi:10.1523/JNEUROSCI.08-02-00395.1988

Catterall WA. 2000. From ionic currents to molecular mechanisms: the structure and function of voltage-gated sodium channels. *Neuron* **26:** 13–25. doi:10.1016/S0896-6273(00)81133-2

Chen X, Wanggou S, Bodalia A, Zhu M, Dong W, Fan JJ, Yin WC, Min H-K, Hu M, Draghici D, et al. 2018. A feedforward mechanism mediated by mechanosensitive ion channel PIEZO1 and tissue mechanics promotes glioma aggression. *Neuron* **100:** 799–815.e7. doi:10.1016/j.neuron.2018.09.046

Chopra SS, Stroud DM, Watanabe H, Bennett JS, Burns CG, Wells KS, Yang T, Zhong TP, Roden DM. 2010. Voltage-gated sodium channels are required for heart development in zebrafish. *Circ Res* **106:** 1342–1350. doi:10.1161/CIRCRESAHA.109.213132

Daul AL, Komori H, Lee C-Y. 2010. EdU (5-ethynyl-2′-deoxyuridine) labeling of *Drosophila* mitotic neuroblasts. *Cold Spring Harb Protoc* **2010:** pdb.prot5461. doi:10.1101/pdb.prot5461

Doe CQ. 2008. Neural stem cells: balancing self-renewal with differentiation. *Development* **135:** 1575–1587. doi:10.1242/dev.014977

Eijkelkamp N, Linley JE, Baker MD, Minett MS, Cregg R, Werdehausen R, Rugiero F, Wood JN. 2012. Neurological perspectives on voltage-gated sodium channels. *Brain* **135:** 2585–2612. doi:10.1093/brain/aws225

Farnsworth DR, Doe CQ. 2017. Opportunities lost and gained: changes in progenitor competence during nervous system development. *Neurogenesis (Austin)* **4:** e1324260. doi:10.1080/23262133.2017.1324260

Feng G, Deák P, Chopra M, Hall LM. 1995. Cloning and functional analysis of TipE, a novel membrane protein that enhances *Drosophila para* sodium channel function. *Cell* **82:** 1001–1011. doi:10.1016/0092-8674(95)90279-1

Francis KR, Wei L, Yu SP. 2015. SRC tyrosine kinases regulate neuronal differentiation of mouse embryonic stem cells via modulation of voltage-gated sodium channel activity. *Neurochem Res* **40:** 674–687. doi:10.1007/s11064-015-1514-4

Fraser SP, Diss JKJ, Chioni A-M, Mycielska ME, Pan H, Yamaci RF, Pani F, Siwy Z, Krasowska M, Grzywna Z, et al. 2005. Voltage-gated sodium channel expression and potentiation of human breast cancer metastasis. *Clin Cancer Res* **11:** 5381–5389. doi:10.1158/1078-0432.CCR-05-0327

Ganetzky B. 1984. Genetic studies of membrane excitability in *Drosophila*: lethal interaction between two temperature-sensitive paralytic mutations. *Genetics* **108:** 897–911.

Ganetzky B, Wu CF. 1982. Indirect suppression involving behavioral mutants with altered nerve excitability in *DROSOPHILA MELANOGASTER*. *Genetics* **100:** 597–614.

Harris JB, Pollard SL. 1986. Neuromuscular transmission in the murine mutants "motor end-plate disease" and "jolting". *J Neurol Sci* **76:** 239–253. doi:10.1016/0022-510X(86)90172-3

He L, Si G, Huang J, Samuel ADT, Perrimon N. 2018. Mechanical regulation of stem-cell differentiation by the stretch-activated Piezo channel. *Nature* **555:** 103–106. doi:10.1038/nature25744

Homem CCF, Knoblich JA. 2012. *Drosophila* neuroblasts: a model for stem cell biology. *Development* **139:** 4297–4310. doi:10.1242/dev.080515

Homem CCF, Repic M, Knoblich JA. 2015. Proliferation control in neural stem and progenitor cells. *Nat Rev Neurosci* **16:** 647–659. doi:10.1038/nrn4021

Huang X, Dubuc AM, Hashizume R, Berg J, He Y, Wang J, Chiang C, Cooper MK, Northcott PA, Taylor MD, et al. 2012. Voltage-gated potassium channel EAG2 controls mitotic entry and tumor growth in medulloblastoma via regulating cell volume dynamics. *Genes Dev* **26:** 1780–1796. doi:10.1101/gad.193789.112

Huang X, He Y, Dubuc AM, Hashizume R, Zhang W, Reimand J, Yang H, Wang TA, Stehbens SJ, Younger S, et al. 2015. EAG2 potassium channel with evolutionarily conserved function as a brain tumor target. *Nat Neurosci* **18:** 1236–1246. doi:10.1038/nn.4088

Hutterer A, Betschinger J, Petronczki M, Knoblich JA. 2004. Sequential roles of Cdc42, Par-6, aPKC, and Lgl in the establishment of epithelial polarity during *Drosophila* embryogenesis. *Dev Cell* **6:** 845–854. doi:10.1016/j.devcel.2004.05.003

Jiang Y, Reichert H. 2012. Programmed cell death in type II neuroblast lineages is required for central complex development in the *Drosophila* brain. *Neural Dev* **7:** 3. doi:10.1186/1749-8104-7-3

Kim K, Hung R-J, Perrimon N. 2017. miR-263a regulates ENaC to maintain osmotic and intestinal stem cell homeostasis in *Drosophila*. *Dev Cell* **40:** 23–36. doi:10.1016/j.devcel.2016.11.023

Lee T, Lee A, Luo L. 1999. Development of the *Drosophila* mushroom bodies: sequential generation of three distinct types of neurons from a neuroblast. *Development* **126:** 4065–4076.

Li D, Zou X-Y, El-Ayachi I, Romero LO, Yu Z, Iglesias-Linares A, Cordero-Morales JF, Huang GT-J. 2019. Human dental pulp stem cells and gingival mesenchymal stem cells display action potential capacity in vitro after neuronogenic differentiation. *Stem Cell Rev Rep* **15:** 67–81. doi:10.1007/s12015-018-9854-5

Lin W-H, Wright DE, Muraro NI, Baines RA. 2009. Alternative splicing in the voltage-gated sodium channel $DmNa_v$ regulates activation, inactivation, and persistent current. *J Neurophysiol* **102:** 1994–2006. doi:10.1152/jn.00613.2009

Loedige I, Jakob L, Treiber T, Ray D, Stotz M, Treiber N, Hennig J, Cook KB, Morris Q, Hughes TR, et al. 2015. The crystal structure of the NHL domain in complex with RNA reveals the molecular basis of *Drosophila* brain-tumor-mediated gene regulation. *Cell Rep* **13:** 1206–1220. doi:10.1016/j.celrep.2015.09.068

McLaughlin KA, Levin M. 2018. Bioelectric signaling in regeneration: mechanisms of ionic controls of growth and form. *Dev Biol* **433:** 177–189. doi:10.1016/j.ydbio.2017.08.032

Olson RO, Liu Z, Nomura Y, Song W, Dong K. 2008. Molecular and functional characterization of voltage-gated sodium channel variants from *Drosophila melanogaster*. *Insect Biochem Mol Biol* **38:** 604–610. doi:10.1016/j.ibmb.2008.01.003

Parker L, Padilla M, Du Y, Dong K, Tanouye MA. 2011. *Drosophila* as a model for epilepsy: *bss* is a gain-of-function mutation in the para sodium channel gene that leads to seizures. *Genetics* **187:** 523–534. doi:10.1534/genetics.110.123299

Parks AL, Cook KR, Belvin M, Dompe NA, Fawcett R, Huppert K, Tan LR, Winter CG, Bogart KP, Deal JE, et al. 2004. Systematic generation of high-resolution deletion coverage of the *Drosophila melanogaster* genome. *Nat Genet* **36:** 288–292. doi:10.1038/ng1312

Patel F, Brackenbury WJ. 2015. Dual roles of voltage-gated sodium channels in development and cancer. *Int J Dev Biol* **59:** 357–366. doi:10.1387/ijdb.150171wb

Planells-Cases R, Caprini M, Zhang J, Rockenstein EM, Rivera RR, Murre C, Masliah E, Montal M. 2000. Neuronal death and perinatal lethality in voltage-gated sodium channel α_{II}-deficient mice. *Biophys J* **78:** 2878–2891. doi:10.1016/S0006-3495(00)76829-9

Pusch M, Noda M, Stühmer W, Numa S, Conti F. 1991. Single point mutations of the sodium channel drastically reduce the pore permeability without preventing its gating. *Eur Biophys J* **20:** 127–133. doi:10.1007/BF01561134

Smith MR, Goldin AL. 1997. Interaction between the sodium channel inactivation linker and domain III S4-S5. *Biophys J* **73:** 1885–1895. doi:10.1016/S0006-3495(97)78219-5

Smith RS, Kenny CJ, Ganesh V, Jang A, Borges-Monroy R, Partlow JN, Hill RS, Shin T, Chen AY, Doan RN, et al. 2018. Sodium channel SCN3A (NaV1.3) regulation of human cerebral cortical folding and oral motor development. *Neuron* **99:** 905–913.e7. doi:10.1016/j.neuron.2018.07.052

Song Y, Lu B. 2011. Regulation of cell growth by Notch signaling and its differential requirement in normal vs. tumor-forming stem cells in *Drosophila*. *Genes Dev* **25:** 2644–2658. doi:10.1101/gad.171959.111

Song M, Mohamad O, Chen D, Yu SP. 2013. Coordinated development of voltage-gated Na^+ and K^+ currents regulates functional maturation of forebrain neurons derived from human induced pluripotent stem cells. *Stem Cells Dev* **22:** 1551–1563. doi:10.1089/scd.2012.0556

Stessman HAF, Xiong B, Coe BP, Wang T, Hoekzema K, Fenckova M, Kvarnung M, Gerdts J, Trinh S, Cosemans N, et al. 2017. Targeted sequencing identifies 91 neurodevelopmental-disorder risk genes with autism and developmental-disability biases. *Nat Genet* **49:** 515–526. doi:10.1038/ng.3792

Subramanian N, Wetzel A, Dombert B, Yadav P, Havlicek S, Jablonka S, Nassar MA, Blum R, Sendtner M. 2012. Role of $Na_v1.9$ in activity-dependent axon growth in motoneurons. *Hum Mol Genet* **21:** 3655–3667. doi:10.1093/hmg/dds195

Tseng A-S, Beane WS, Lemire JM, Masi A, Levin M. 2010. Induction of vertebrate regeneration by a transient sodium current. *J Neurosci* **30:** 13192–13200. doi:10.1523/JNEUROSCI.3315-10.2010

Wallace K, Liu TH, Vaessin H. 2000. The pan-neural bHLH proteins DEADPAN and ASENSE regulate mitotic activity and cdk inhibitor *dacapo* expression in the *Drosophila* larval optic lobes. *Genesis* **26:** 77–85. doi:10.1002/(SICI)1526-968X(200001)26:1<77::AID-GENE10>3.0.CO;2-R

Warmke JW, Reenan RA, Wang P, Qian S, Arena JP, Wang J, Wunderler D, Liu K, Kaczorowski GJ, Van der Ploeg LH, et al. 1997. Functional expression of *Drosophila para* sodium channels. modulation by the membrane protein TipE and toxin pharmacology. *J Gen Physiol* **110:** 119–133. doi:10.1085/jgp.110.2.119

Xia J, Huang N, Huang H, Sun L, Dong S, Su J, Zhang J, Wang L, Lin L, Shi M, et al. 2016. Voltage-gated sodium channel $Na_v1.7$ promotes gastric cancer progression through MACC1-mediated upregulation of NHE1. *Int J Cancer* **139:** 2553–2569. doi:10.1002/ijc.30381

Xu C, Luo J, He L, Montell C, Perrimon N. 2017. Oxidative stress induces stem cell proliferation via TRPA1/RyR-mediated Ca2+ signaling in the *Drosophila* midgut. *Elife* **6:** e22441. doi:10.7554/eLife.22441

Yamamoto S, Jaiswal M, Charng W-L, Gambin T, Karaca E, Mirzaa G, Wiszniewski W, Sandoval H, Haelterman NA, Xiong B, et al. 2014. A *Drosophila* genetic resource of mutants to study mechanisms underlying human genetic diseases. *Cell* **159:** 200–214. doi:10.1016/j.cell.2014.09.002

Yang M, Kozminski DJ, Wold LA, Modak R, Calhoun JD, Isom LL, Brackenbury WJ. 2012. Therapeutic potential for phenytoin: targeting $Na_v1.5$ sodium channels to reduce migration and invasion in metastatic breast cancer. *Breast Cancer Res Treat* **134:** 603–615. doi:10.1007/s10549-012-2102-9

Younger-Shepherd S, Vaessin H, Bier E, Jan LY, Jan YN. 1992. *deadpan*, an essential pan-neural gene encoding an HLH protein, acts as a denominator in *Drosophila* sex determination. *Cell* **70:** 911–922. doi:10.1016/0092-8674(92)90242-5

Yu FH, Mantegazza M, Westenbroek RE, Robbins CA, Kalume F, Burton KA, Spain WJ, McKnight GS, Scheuer T, Catterall WA. 2006. Reduced sodium current in GABAergic interneurons in a mouse model of severe myoclonic epilepsy in infancy. *Nat Neurosci* **9:** 1142–1149. doi:10.1038/nn1754

Zhu S, Wildonger J, Barshow S, Younger S, Huang Y, Lee T. 2012. The bHLH repressor deadpan regulates the self-renewal and specification of *Drosophila* larval neural stem cells independently of notch. *PLoS One* **7:** e46724. doi:10.1371/journal.pone.0046724

Paralytic, the *Drosophila* voltage-gated sodium channel, regulates proliferation of neural progenitors

Beverly J. Piggott, Christian J. Peters, Ye He, et al.

Genes Dev. 2019, **33:** originally published online November 21, 2019
Access the most recent version at doi:10.1101/gad.330597.119